Measurement of Passive R, L, and C Components Under Nonsinusoidal Conditions: The Solution of Some Case Studies

Luigi Ferrigno, *Member, IEEE*, Marco Laracca, *Member, IEEE*, and Antonio Pietrosanto, *Member, IEEE*

***Abstract*—This paper deals with the measurement of the R, L, and C parameters of passive components in nonsinusoidal conditions. Since these components usually work with voltage and current waveforms that are different from sinusoidal ones, nonsinusoidal characterization has to be made. The importance of nonsinusoidal characterization of passive components is highlighted through the analysis of two case studies: 1) the influence of distorted waveforms on the Line Impedance Stabilizer Network (LISN) passive component behaviors and 2) the influence of voltage and current harmonics on hybrid filter responses. In this paper, the authors propose and describe a measurement method based on linear system identification and model parameter estimation techniques. Then, the two case studies are analyzed and described with the help of some test results.**

***Index Terms*—Equivalent circuits, identification, impedance measurement, nonsinusoidal characterization, RLC circuits.**

I. Introduction

TODAY, electric and electronic devices working with signals characterized by a high harmonic content are so widespread that sinusoidal conditions can be established neither inside nor outside of them. This means that both their own components (e.g., resistors, inductors, capacitors, varistors, insulated gate bipolar transistors, and field-effect transistors) [1], [3] and devices dealing with them (e.g., motors [4]–[6], filters [7], and power cables) all work with wideband voltage and current signals. Moreover, the need for compactness and performance in power and consumer electronics has led to an increase in the following: 1) the operation frequency; 2) the integration of passive components onto printed circuit boards; and 3) the use of nonsinusoidal signals. In this framework, the higher the clock and switching circuit frequencies, the more there will be factors that influence passive components, thus making their behavior unpredictable. Effects such as dielectric or magnetic nonlinearity, hysteresis, eddy currents, and self-resonance can make the passive component choice a hard task for system designers.

Manuscript received April 23, 2007; revised March 22, 2008. First published May 30, 2008; current version published October 10, 2008.

L. Ferrigno and M. Laracca are with the Department of Automation, Electromagnetism, Information Engineering, and Industrial Mathematics (DAEIMI), University of Cassino, 03043 Cassino, Italy (e-mail: ferrigno@unicas.it; m.laracca@unicas.it).

A. Pietrosanto is with the Department of Electrical and Information Engineering (DIIIE), University of Salerno, 84084 Salerno, Italy (e-mail: apietrosanto@unisa.it).

Color versions of one or more of the figures in this paper are available online at http://ieeexplore.ieee.org.

Digital Object Identifier 10.1109/TIM.2008.924927

In some cases, suitable international standards precisely define both system equivalent circuits (whose R, L, and C are time-invariant parameters) and modalities and tests to evaluate their parameters [2], [3]. These rules or conventions allow the following: 1) comparison among products made in different places; 2) quality control; and 3) nominal performance characterization. Depending on both systems and applications, the significance of the circuit and its parameters can be different, but it is clear that designers are used to assign a value to R, L, and C parameters either by impedance measurement or by standard tests made in sinusoidal conditions.

With most of these components being nonlinear, a parameter estimation based on a sinusoidal stimulus should be considered to be quite approximate. Nevertheless, in rough circuit analysis, R, L, and C parameters are continuously being considered substantially invariant with respect to the voltage or current waveform. Nonsinusoidal conditions are eventually held into account by expanding the uncertainty of the parameters on the basis of impedance measurements carried out in all the frequency bands of the input signal by either an RLC meter or a network analyzer [6], [7]. On the contrary, in all applications where these electric and electronic devices must be designed so that system characteristics (e.g., output signal distortion, input and output impedance, and output voltage amplitude) are constrained in known and narrow ranges, R, L, and C parameters cannot be known with such an uncertainty, and an *ad hoc* measurement method is strongly required.

With this aim, in a previous work [8], the authors proposed a parameter estimation technique as the basis of a new R, L, and C measurement method that is particularly useful when the aforementioned components operate under nonsinusoidal conditions. This technique was described in detail and tested for both sinusoidal and nonsinusoidal signals, but its performance was only evaluated for the first-order models of the passive components. Starting from these considerations and limits, this paper presents the extension of the measurement method to the second- and higher order models. The proposed step is not trivial since increasing the model order swells the measurement method complexity, the required accuracy in the identification phase, and the difficulty in the parameter estimation phase much more.

Furthermore, the improved technique has been tested on two case studies, which will be presented in Sections III and IV. The first concerns the characterization of a Line Impedance Stabilizer Network (LISN), whereas the second concerns the

0018-9456/$25.00 © 2008 IEEE

characterization of a hybrid filter for power quality assessment. These two cases are very important for two reasons.

1) The LISN behavior in nonsinusoidal conditions is different than expected. Thus, it is possible to reduce the related uncertainty only through the LISN characterization made in the actual test conditions.
2) Given the functionality of the active module in hybrid filters as strongly dependent on the behavior of the passive module, an inaccurate calibration of this last part significantly decreases the hybrid filter performance.

II. Measurement Method

To give a value to R, L, and C parameters of a system equivalent circuit, the authors propose a method [8] that is based on a linear system model parameter estimation technique. It is well known from the parameter estimation theory [9] that once a linear system model structure has been identified, the model parameters can be estimated through an elaboration of system input and output signals. The resulting parametric model will reproduce the output–input relationship, regardless of the input signal, only if some specific conditions have been satisfied during the parameter-estimation phase. The most important condition is that the system must be linear. Otherwise, the model parameter values will characterize the system behavior only if the input signal is the same as that used for the parameter estimation. If the input signal is changed, then a new parameter estimation is required to provide new system model parameters. Moving from the general estimation problem to the R, L, and C parameter estimation under nonsinusoidal conditions, the aforementioned considerations drove the authors to conclude the following.

1) Once both the equivalent circuit and the operative conditions (shapes of the voltage and current waveforms, temperature, etc.) of a nonlinear system have been defined, it must be seen as a single-input–single-output (SISO) linear time-invariant (LTI) system whose transfer function $H(z)$ is obtained by the equivalent circuit in the system identification phase.
2) For a given SISO LTI system, using an output-error (OE) model, it is possible to write $y(k) = w(k) + e(k)$, where $y(k)$, $w(k)$, and $e(k)$ are the kth samples of the system output, the undisturbed output, and the output additive error, respectively.
3) The relation between the input $x(k)$ and the undisturbed output $w(k)$ can be written in the discrete-time domain as $w(k)+\theta_0 w(k-1)+\cdots+\theta_{nf-1}w(k-nf)=\theta_{nf}x(k-nk)+\cdots+\theta_{nf+nb}x(k-nk-nb)$, where the θ_i coefficients are time-independent model parameters.
4) Moving from the discrete-time domain to the z-domain, letting $X(z), Y(z)$, and $E(z)$ be the z-transforms of $x(k)$, $y(k)$, and $e(k)$, respectively, $H(z)$ is the system transfer function, and nk is the delay between $w(k)$ and $x(k)$, it is possible to write $Y(z) = H(z)X(z) + E(z)$, where

$$H(z) = \frac{\theta_{nf}z^{-nk} + \cdots + \theta_{nf+nb}z^{-nk-nb}}{1 + \theta_0 z^{-1} + \cdots + \theta_{nf-1}z^{-nf}}. \quad (1)$$

5) The system models in both the time domain and z-domain are completely defined by knowledge of the parameter set $\{\theta_i\}$. It is worth remarking that the $\{\theta_i\}$ parameters allow the system behavior to be reproduced only in the operative condition of the parameter estimation phase. If this condition changes, a new parametric estimation is required.

The $\{\hat{\theta}_i\}$ estimation of $\{\theta_i\}$ parameters is conducted using an optimization procedure, as explained in [8]. Finally, for the given equivalent circuit, the corresponding R, L, and C parameters are calculated from $\{\hat{\theta}_i\}$. In [8], only the first-order models were implemented and extensively tested.

Some details and steps of the measurement procedure have to be improved to allow the higher order models to be implemented. In fact, to increase the order of the estimated model, some changes are necessary in 1) the identification of the $H(z)$ transfer function and 2) the relationships to be used in the calculation of the R, L, and C parameter values from $\{\hat{\theta}_i\}$.

As far as item 1) is concerned, the crucial point is the transformation from the continuous $(H(s))$ representation of the model to the discrete $(H(z))$ transfer function. This can be executed according to various strategies as zero-order hold (ZOH), first-order hold, pole-zero matching (PZM), bilinear with and without prewarping, step invariance method, etc. Each method leads to a different shape of the $H(z)$ transfer function and, consequently, to a different relationship in the parameter estimation phase. After a detailed analysis carried out in a mathematical simulation environment, the best continuous-to-discrete transformation method has been determined for each model order.

As for item 2), a further problem arises in the estimation of the R, L, and C parameters since the analytical relationship involves the solution of the second- and third-order equations. For these reasons, more solutions are mathematically allowed, but only one is right. Therefore, during the parameter-estimation phase, some constraints must be imposed to the analytical solutions.

As an example, Table I reports the schematic of some equivalent circuits that are usually suggested for resistors, capacitors, and inductors when nonlinear dielectric or magnetic effects are caused by high operating voltages or currents (both the principal and parasitic R, L, and C parameters that compose these equivalent circuits are frequency dependent). All these equivalent circuits give rise to the second-order models in the z-domain.

To better describe the measurement procedure, as an example, once a suitable model has been chosen in Table I(c), the following equation can be written for a real capacitor:

$$G(s) = \frac{I(s)}{V(s)} = \frac{\frac{1}{R+R'} * (sCR+1)}{\frac{LCR}{R+R'}s^2 + \frac{L}{R+R'}s + 1} = \frac{G * (1+sT_3)}{(1+sT_0) * (1+sT_1)}. \quad (2)$$

The associated discrete model that adopts a PZM continuous-to-discrete transform can be defined as

$$G(z) = \frac{I(z)}{V(z)} = \frac{\theta_2 z^{-1}(1-\theta_3 z^{-1})}{(1-\theta_0 z^{-1}) * (1+\theta_1 z^{-2})} \quad (3)$$

TABLE I
IMPLEMENTED SECOND-ORDER MODELS FOR THE R, L, AND C COMPONENTS

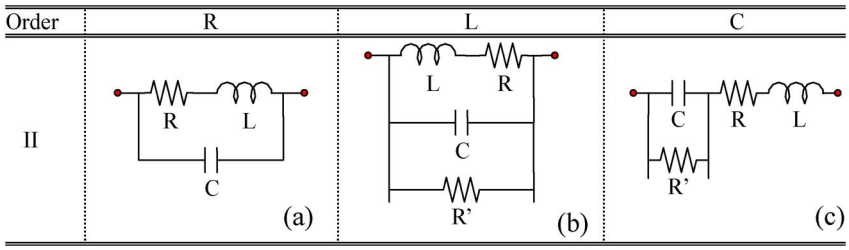

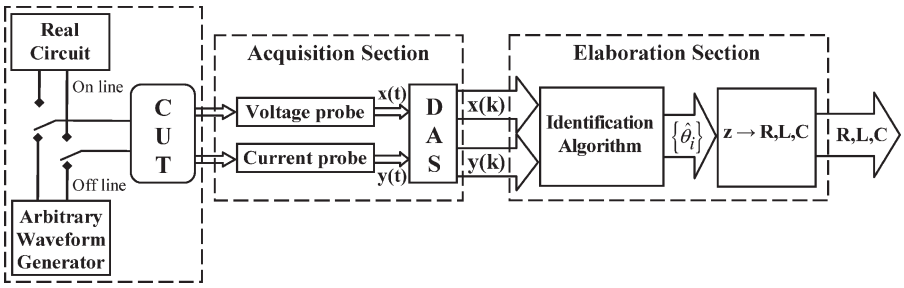

Fig. 1. Operating diagram of the proposed method.

where the relations among the continuous and discrete coefficients are reported as follows:

$$\theta_0 = e^{\frac{-T_c}{T_0}} \quad \theta_1 = e^{\frac{-T_c}{T_1}}$$
$$\theta_1 = e^{\frac{-T_c}{T_2}} \quad \theta_2 = \frac{G(1-\theta_0)(1+\theta_1)}{(1-\theta_3)} \tag{4}$$

with T_c as the discrete sampling time.

Once the $\{\hat{\vartheta}_i\}$, $i = 0, 1, 2, 3$ coefficients have been estimated by the previously described least squares method (LSM) OE parametric estimation method, the relations reported in (4) easily lead to the estimated $\{\hat{R}, \hat{R}', \hat{L}, \hat{C}\}$ coefficients. Fig. 1 shows a functional block diagram of the measurement station based on three main sections: the elaboration section, the acquisition section, and the generation section.

When the component is not embedded in a real circuit, the *generation section* provides arbitrary stimulus voltages or currents to offline measurements by means of an arbitrary waveform generator. The *acquisition section* is dedicated to acquire the input and output signals [$x(t)$ and $y(t)$, respectively] from the circuit under test (CUT). The *elaboration section* runs both signal processing and instrument control software.

As far as the measurement uncertainty is concerned, considering the measurement chain sketched in Fig. 1, five contributors can be highlighted: 1) uncertainty of the adopted signal generator; 2) uncertainties of voltage and current transducers; 3) uncertainty related to the signal-to-noise ratio of the data acquisition systems (DAS); 4) uncertainty of the parameter estimation method; and finally, 5) uncertainty related to the discrete-to-continuous transform required to obtain the R, L, and C parameters starting from the estimated $\{\hat{\vartheta}_i\}$ coefficients. To accurately determine the aforementioned contributors, both systematic errors and repeatability terms should be estimated. Since a reference impedance meter working in nonsinusoidal conditions is not yet available on the market, a comparison with the estimated R, L, and C values to evaluate the systematic effects cannot be made. For these reasons, the repeatability of the measurement method was only estimated using a statistical approach.

TABLE II
NOMINAL VALUES AND MAXIMUM VOLTAGE AND CURRENT FOR THE SELECTED COMPONENTS

	R	L	C
Nominal Value	1 Ω	0.7 mH	22 μF
V_{MAX} (RMS)	10 V	250 V	270 V
I_{MAX} (RMS)	10 A	4 A	10 A

In particular, the overall acquired voltage and current signals have been divided into 50 nonoverlapping sequences. The total acquired record length was set to 100 kS, whereas each subsequence was 2 kS long. Furthermore, the parametric estimation measurement method was applied to each of the realized subsequences, obtaining a mean value and a standard deviation for the estimated $\{\hat{\vartheta}_i\}$ coefficients. This allowed the uncertainty propagation law [10] to be applied to the analytical expression of the R, L, and C parameters to calculate the standard uncertainty of each component (i.e., u_R, u_L, and u_C) due to the casual variability of the estimated $\{\hat{\vartheta}_i\}$ coefficients.

Applying the previously described measurement method, for testing purposes, a ceramic resistor, an electrolytic capacitor, and an air-wound inductor were used. The nominal value and the maximum root-mean-square (rms) voltage and current applied to each component are reported in Table II. These values represent the operative voltage and current conditions that are very near the allowed component limits. As far as the system identification phase is concerned, a ZOH transformation was adopted to pass from the continuous-to-discrete domain. The parameter estimation phase was carried out with a nonsinusoidal input signal containing six equally spaced tones in the 500- to 1000-Hz range. To characterize the component response for the typical operative working condition, three signals with different amplitudes have been used for the R, L, and C components (the magnitudes and phases of the tones of the used stimulus are reported in Table III). Once a set of $\{\theta_i\}$

TABLE III
RESULTS OBTAINED ON SOME PASSIVE COMPONENTS USING A NONSINUSOIDAL STIMULUS WITH SIX EQUISPACED TONES IN THE 500- TO 1000-Hz RANGE SINUSOIDAL STIMULUS AND OPERATING CURRENTS NEAR THE MAXIMUM ALLOWED

Comp.	Stimulus signal			Used Model	Err	L [μH] $\dot{u}_L$	R [Ω] $\dot{u}_R$	C [μF] $\dot{u}_C$	R' [Ω] $\dot{u}_{R'}$
	V_{RMS} [V] all tones	Phase [°] all tones	I_{RMS}[A] V_{RMS}[V]						
R	1.39	0	2.5 3.4	a)	0.022	7.015 0.050	1.300 0.018	0.867 0.047	N/A
L	5.06	0	3.0 12.4	b)	0.055	660.57 0.069	0.037 0.070	0.987 0.050	97.87 0.073
C	12.57	0	4.2 30.8	c)	0.040	4.47 0.086	72.84 0.010	22.08 0.014	0.129 0.022

parameters was obtained for each component, the R, L, and C parameter calculation was made by imposing constraints to the nth-order equation system as discharge R, L, and C negative solutions and discharge intermediate solutions that lead to complex R, L, and C solutions. The obtained results are reported in Table III, whereas detailed information about the measurement procedure will be given in Section III-B. The measurement uncertainty has been estimated by taking into account the measurement procedure repeatability, the voltage and current probe accuracy, and the quantization errors of the used digital scope.

Since a reference measurement instrument that is capable of working with the same operating currents and voltages is not yet present on the market, the same Err coefficient proposed in [9] was used to quantify the goodness of the estimation procedure. The Err coefficient represents the relative difference between the measured and the estimated output obtained using the calculated $H(z)$ transfer function, i.e.,

$$\mathrm{Err} = \frac{1}{\max\left(|y(k)|\right) \cdot N} \sum_{k=1}^{N} \left|\hat{y}(k) - y(k)\right|. \tag{5}$$

In all the tests, its value did not exceed a 0.055 threshold.

The test results show that due to these enhancements, the goodness of the measurement method is also confirmed when higher than first-order models are used.

III. CASE STUDY: NONSINUSOIDAL SIGNALS INFLUENCE THE RESPONSE OF LISNs

A. LISN Presentation and Problems

LISNs are used in conducted disturbance measurements for reproducibility and standard experiments. For standard measurements, the LISN is inserted between the power supply and the equipment under test (EUT) [11]. During the conducted emissions, the following important test features are requested from an LISN:

1) constant impedance versus frequency;
2) concentration of high-frequency conducted disturbances to an ac monitor point;
3) isolation of the EUT from interference coming from an external power source.

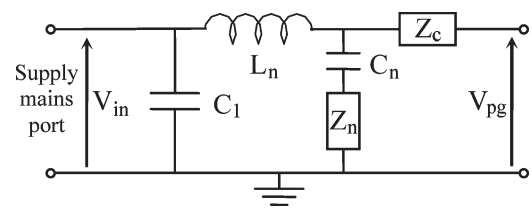

Fig. 2. Single-cell LISN structure.

These features allow site-to-site measurement reproducibility. Different electromagnetic compatibility (EMC) standards, such as FCC [12] and CISPR [13], specify the disturbance limits, frequency range, device class, measuring apparatus, and measurement methods.

Two frequency bands A (low) and B (high) have to be considered, but their ranges change from a standard to another. As far as the LISN structure is concerned, several topologies are allowed. For each band, the required behavior is obtained by adopting different LISN topologies and, consequently, different passive components. The simplest LISN topology is the single-cell structure shown in Fig. 2, where V_{in} is the exciting power supply voltage, and V_{pg} is the common-mode disturbance.

In the low-frequency range, inductors L_n must provide a low-impedance path for the ac power, whereas capacitors C_n and C_1 must provide a high-impedance path to reduce leakage currents but not to overload the measurement resistors. In the high-frequency range, capacitor C_1 and inductors L_n act as a filter and divert external noise. Capacitor C_n and resistor Z_n provide a specific path for measured disturbances with constant impedance versus frequency.

Considering band A, the single LISN cell topology cannot always be used. To perform efficient external noise filtering, the CISPR LISN requires greater input inductors due to the lower frequency range. This adds up to slightly more complex topologies. A classical single cell can be used with more specific Z_n impedance, or a two-cell topology can be considered (Fig. 3).

The desired LISN characteristic impedance is defined by standards. It can be described by a parallel between a 50-Ω resistor and a 50-μH inductor, in series with a 5-Ω resistor [13]. The corresponding operating characteristic of the impedance modulus is given in Fig. 4. Standards specify the maximum allowed accuracy for the LISN modulus impedance, within the 20% range of the nominal operating characteristics, whereas no indication is given for the phase.

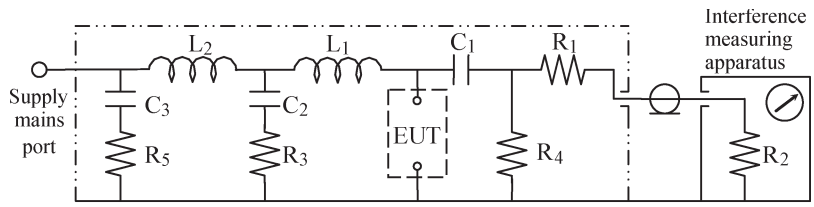

R1+R2	50 Ω	**R5**	10 Ω	**C1**	0.25 μF
R3	5 Ω	**L1**	50 μH	**C2**	8 μF
R4	1 kΩ	**L2**	250 μH	**C3**	1.2 μF

Fig. 3. General structure of a double-cell LISN together with the nominal values of its components.

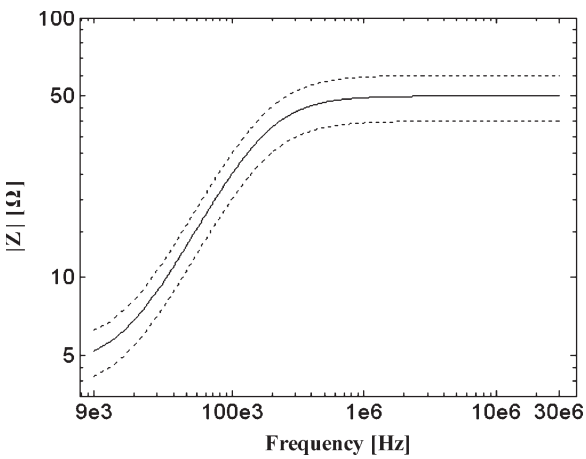

Fig. 4. LISN impedance modulus characteristic according to the (solid line) CISPR norm and (dashed line) allowed accuracy.

Previous works [14]–[16] pay attention to the definition of the LISN parameters. In particular, they show that low accuracy leads to high uncertainty in the conducted disturbance measurements [17] and that many problems arise even if the LISN is constructed according to EMC standard specifications. In fact, the LISN behavior depending on the manufacturer can cause variability of the EUT conducted emission measurements in the range from 10 to 20 dB [14]. This is a serious problem if site-to-site measurement reproducibility and EUT acceptability have to be granted.

Furthermore, the previously mentioned CISPR16-1 gives stringent requirements on the nominal impedance LISN modulus, whereas no specifications are given about the impedance LISN phase (θ). Other papers [16] show that by varying the phase value, significant errors can be noted in the conducted emission measurements. It is clear that phase variations depend on the presence of several parasitic parameters, which, in turn, depend on the frequency range and waveform topology, and this dependence has not been taken into account in the CISPR model. Several experiments showed that it is possible to have compliance between the CISPR16-1 requirements and the LISN modulus but with a wide phase variation range [19]. This is a supplementary and undesired contributor to the conducted emission measurement uncertainty that has to be added to that introduced by the CISPR standard. In the next section, the measurement method proposed in Section II is used to characterize the LISN behavior using the same noisy signals present during the EMC tests. It will be shown that this new characterization may significantly reduce the measurement uncertainty due to the LISN parameters.

TABLE IV
IMPLEMENTED FIRST- AND SECOND-ORDER LISN MODELS

Order	Model
I	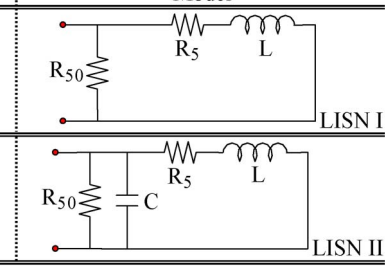
II	

B. Measurement Procedure

A brief description of the realized measurement procedure is given in the following. Let us start from the LISN I model reported in Table IV. With reference to the voltage applied to the R_{50} resistance and the incoming current, the LISN transfer function can be defined as

$$H(s) = \frac{V(s)}{I(s)} = \frac{R_{50} * \left(s + \frac{R_5}{L}\right)}{s + \frac{(R_{50}+R_5)}{L}}. \tag{6}$$

The associated discrete model that adopts a ZOH continuous-to-discrete transform can be obtained as

$$H(z) = \frac{\theta_1 - \theta_2 z^{-1}}{1 - \theta_0 z^{-1}} \tag{7}$$

where the relations among the continuous and discrete coefficients are reported as follows:

$$\begin{aligned} \theta_0 &= e^{\frac{-T_c(R_{50}+R_5)}{L}} \\ \theta_1 &= R_{50} \\ \theta_2 &= \theta_1 + (\theta_0 - 1)\frac{R_{50} * R_5}{R_{50} + R_5} \end{aligned} \tag{8}$$

with T_c as the discrete sampling time.

Once the $\{\hat{\vartheta}_i\},\ i = 0, 1, 2$ coefficients have been estimated by the previously described LSM OE parametric estimation method, the relations reported in (8) easily lead to the estimated $\{\hat{R}_{50}, \hat{R}_5, \hat{L}\}$ coefficients.

As far as the measurement uncertainty is concerned, some considerations reported in the previous section can be applied.

TABLE V
ESTIMATED VALUES OF THE LISN PASSIVE COMPONENTS AND ERR COEFFICIENTS FOR THE SELECTED MODELS OF THE FIRST TEST

Used Model		Err	R50 [Ω]	R5 [Ω]	L [μH]	C [nF]
LISN I	Component value	0.15	9.54	1.55	125.5	N/A
	Rel. unc.	--	0.025	0.25	0.082	
LISN II	Component value	0.14	10.28	1.71	117.2	51.77
	Rel. unc.	--	0.050	0.050	0.053	0.037

C. Experimental Results

The experimental tests were carried out on an AFJ LT32 double-cell LISN. This LISN is manufactured according to the CISPR standard. Its operating range is from 9 kHz to 30 MHz.

The steps reported in Section II were considered, and according to Hall [14] and Crebier *et al.* [15], two simple LISN models were used. The first model describes the same model provided by the CISPR standard and accomplished by the LISN manufacturer, whereas the second model also takes into account parasitic effects through a parallel capacitor. These models are described in Table IV.

Offline tests were carried out using an EM TEST CWS 500A (9 kHz to 240 MHz, 75 W) to generate the stimulus signals. In accordance with the block diagram sketched in Fig. 1, the acquisition section was composed of the following: 1) an IEEE-488 controlled digital oscilloscope (Tektronix TDS 540D, 500 MHz bandwidth, four-input single-ended channels, maximum 1 GS/s sampling frequency for each channel, total record length of 8 MS, from 8- to 15-bit resolution in the high-resolution mode) used as the DAS; 2) an active current probe (Tektronix TCP202, 0–50 MHz bandwidth, 15 A dc + peak ac); and 3) a passive voltage probe (Agilent Technologies 10070C, 20 MHz bandwidth, attenuation ratio 1 : 1).

In the first test, a multisine waveform was used as the exciting voltage. Its rms value was 300 mV, and its harmonic range was composed of 11 equally spaced sinusoids in the 10- to 20-kHz range. All tones had the same magnitude (equal to 90.5 $\mathrm{mV_{rms}}$) and phase (equal to zero). Both the first- and second-order LISN models were used. Table V shows the obtained results in terms of the component values, the Err coefficients, and the relative standard uncertainty for each estimated component. As can be seen, the obtained values are different from those described in the CISPR norm. To demonstrate the goodness of the identification procedure, as described in [8], the Err coefficient was also estimated using the component nominal values described by the CISPR requirements. The calculated value was 0.82, which is four times greater than that obtained from the parameter estimation process. Two considerations can be made from Table V: 1) The LISN II model better approximates the real behavior due to the presence of parasitic effects; and 2) as shown in Fig. 5, the estimated LISN phase (computed on the estimated R, L, and C parameters) is different from that expected from implementing the CISPR model. In particular, Fig. 5 shows the estimated and expected modulus [Fig. 5(a)] and phase [Fig. 5(b)] for the 10- to 20-kHz frequency range covered by the voltage multisine stimulus (for the LISN II case). For the sake of brevity, only the second test was reported. In this case, a noisy voltage multisine stimulus with five tones in the 250-kHz to 2-MHz range was used. In particular, the stimulus signal is composed of tones at the following frequencies: 250 kHz, 500 kHz, 750 kHz, 1 MHz, and 2 MHz. All tones had the same phase (equal to zero) and magnitude (equal to 0.45 $\mathrm{V_{rms}}$). The rms voltage value of the multisine stimulus was about 1 V. The obtained results are reported in Table VI, whereas the estimated and expected transfer function behaviors for the selected input signal are shown in Fig. 6 (for the

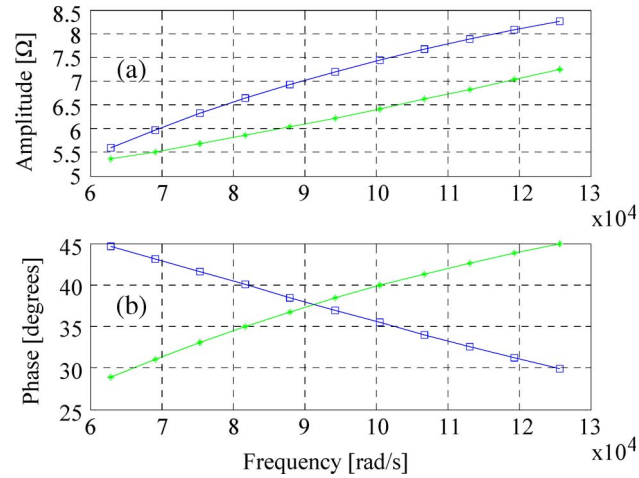

Fig. 5. (Square) estimated and (star) expected LISN impedance (a) amplitudes and (b) phases for the first selected test.

TABLE VI
ESTIMATED VALUES OF THE LISN PASSIVE COMPONENTS AND ERR COEFFICIENTS FOR THE SELECTED MODELS OF THE SECOND TEST

Used Model		Err	R50 [Ω]	R5 [Ω]	L [μH]	C [nF]
LISN I	Component value	0.15	41.90	2.79	47.8	N/A
	Rel. unc.	--	0.0065	0.16	0.045	N/A
LISN II	Component value	0.10	42.884	4.005	46.53	0.1466
	Rel. unc.	--	0.09	0.09	0.10	0.08

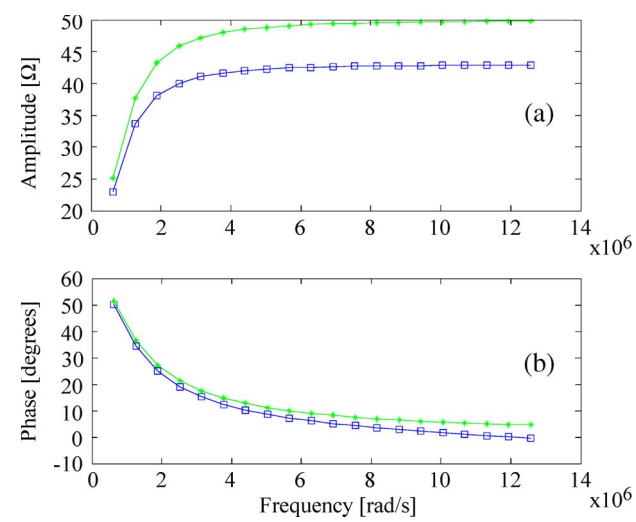

Fig. 6. (Square) estimated and (star) expected LISN impedance (a) amplitudes and (b) phases for the second selected test.

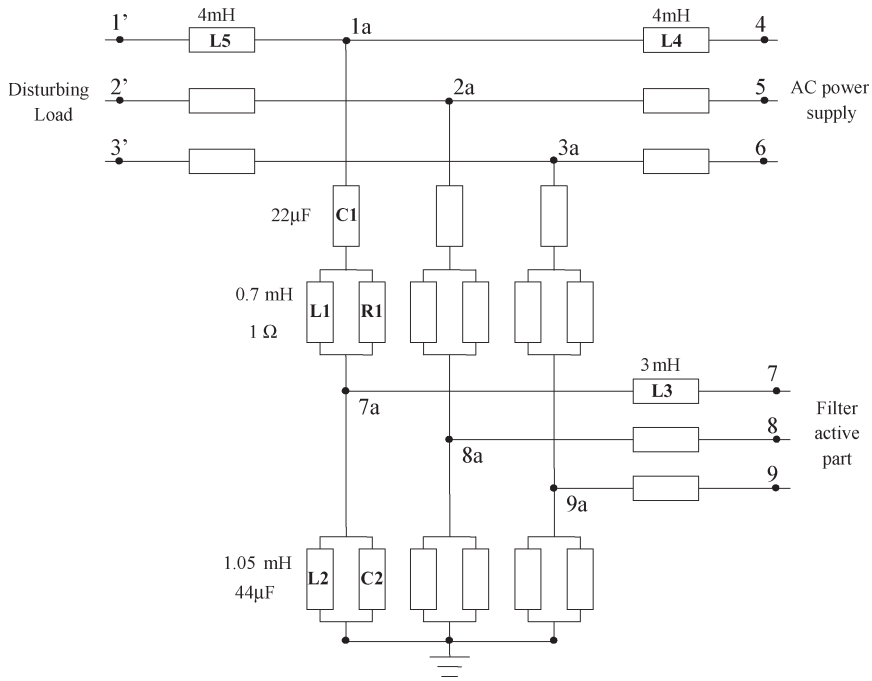

Fig. 7. Architecture of a typical hybrid filter.

LISN II case). Table VI also shows the Err coefficients. The Err coefficient for the imposed CISPR norm parameters is 1.10, which indicates the goodness of the parameter-estimation procedure. As can be seen, in this case, the estimated LISN modulus is different from the expected value in the 250-kHz to 2-MHz frequency range covered by the voltage stimulus.

IV. Second Case Study: How Nonsinusoidal Signals Influence the Behavior of Hybrid Filters

A. Hybrid Filter and Problem Presentation

The proliferation of power electronic loads, such as the three-phase diode and thyristor bridge rectifiers for dc power supplies, adjustable-speed drives, and uninterruptible power systems, which are prerequisites for realizing energy efficiency and productivity benefits, has brought utilities to a crossroads. Utilities frequently encounter harmonic-related problems, including substantially higher transformer and line losses, reactive power and resonance problems, required derating of distribution equipment, and severe harmonic interactions between customers or between the utility and the load. Moreover, harmonic problems reduce electric system stability and its safe operating margins.

To alleviate the harmonic-related problems, utilities are beginning to implement IEEE 519 recommended harmonic standards [18]. Passive filters have traditionally been used to absorb harmonics generated by large industrial loads because of their low cost and high efficiency. These are basically constituted by passive R, L, and C components that act as a low impedance for filtered component harmonics. However, they have several drawbacks; thus, active filters and, successively, hybrid filters were developed. The hybrid filter solution mitigates problems of both active and passive filters and offers several additional features. In particular, this consists of active and passive filters connected, in series or parallel, to each other, thus combining the compensation characteristics of resonant passive and active power filters [18]. In these filters, an active part that is joined with one or more passive filtering networks coupled with the electrical power line is used to generate correcting waveforms that are able to compensate the harmonic disturbances present in the electrical power network. An example of a hybrid filter structure is reported in Fig. 7. The response of the active part of the hybrid filter is strictly related to the response of the coupled R, L, and C passive filter networks [19], [20]. For these reasons, a passive filter response model is implemented in the hybrid filter active part, which is usually a switching circuit. Therefore, model errors may cause, in turn, errors in the hybrid filter response. These errors lead to two effects: 1) The disturbing waveforms are not cancelled from the electrical power line; and 2) new disturbing waveforms are added into the system. The values of the R, L, and C components used in the passive filter model are typically obtained either from datasheets or by using reference impedance meters operating in sinusoidal conditions. Since the R, L, and C passive filters are developed to clean corrupted waveforms, their passive components typically work in nonsinusoidal conditions. In the following section, some experimental results that are involved with the use of the proposed measurement technique to characterize the filter components in the actual operating conditions are presented. The general measurement method described in Section II has been applied for each of the hybrid filter components.

B. Experimental Results

The tests have been done in offline mode using a high-power arbitrary function generator (SIMULBUS) to generate the stimulus signals. The main characteristics of the SIMULBUS are given as follows: 5 kVA maximum output power, 2.5 kHz

TABLE VII
RESULTS OBTAINED ON SOME PASSIVE COMPONENTS OF THE SELECTED HYBRID FILTER USING TWO DIFFERENT NONSINUSOIDAL VOLTAGE STIMULI

Comp.	Used Model	Err	L $\dot{u}_L$ [μH]	R $\dot{u}_R$ [Ω]	C $\dot{u}_C$ [μF]	R' $\dot{u}_{R'}$ [Ω]
MULT1 stimulus						
R1	**a)**	0.10	11.03 0.039	1.308 0.012	1.11 0.040	N/A
L1	**b)**	0.11	680.39 0.047	0.035 0.090	3.314 0.034	60.40 0.047
C1	**c)**	0.090	39.98 0.04	3585 0.09	21.379 0.15	0.38 0.022
MULT2 stimulus						
R1	**a)**	0.062	3.020 0.040	1.320 0.020	0.276 0.035	N/A
L1	**b)**	0.11	658.35 0.069	0.022 0.070	1.744 0.054	57.98 0.073
C1	**c)**	0.055	3.874 0.024	417.9 0.026	21.753 0.038	0.31 0.1

TABLE VIII
CHARACTERISTICS OF THE MULT1 AND MULT2 STIMULUS SIGNALS

MULT1 stimulus							
	Frequencies [Hz]	50	150	350	450	550	--
	Phases [degree]	0	0	0	0	0	--
R_1	Magnitudes [V_{RMS}]	2.60	1.56	1.04	0.65	0.13	--
L_1		1.58	0.94	0.63	0.39	0.08	--
C_1		45.0	27.0	18.0	11.3	2.3	--
MULT2 stimulus							
	Frequencies [Hz]	50	500	600	700	800	1000
	Phases [degree]	0	0	0	0	0	0
R_1	Magnitudes [V_{RMS}]	2.30	1.38	0.92	0.69	0.58	0.12
L_1		4.80	2.88	1.92	1.44	1.20	0.24
C_1		27.0	16.2	10.8	8.10	6.75	1.35

bandwidth, 470 V_{rms} maximum output with 0.4% voltage accuracy, ±5 ppm frequency stability, and the possibility to create arbitrary waveforms using all the frequencies that are multiples of the 16- to 66-Hz fundamental harmonic. The acquisition section is the same as that described in Section III-C, with the only difference being the use of a high-voltage differential probe (Tektronix P5205, 5 MHz bandwidth, attenuation ratios 50 : 1 and 500 : 1).

The experimental tests have been executed on the hybrid filter sketched in Fig. 7, where the nominal values of components are also reported. Table VII shows the tests made on the R_1, L_1, and C_1 components of Fig. 7 obtained, applying to each of them the second-order model shown in Table I. In particular, Table VII shows the two experimental test results obtained with the two voltage waveforms whose harmonic contents are given as follows: 1) fundamental, third, seventh, ninth, and 11th harmonics; and 2) fundamental, 10th, 12th, 14th, 16th, and 20th harmonics. They are also called mult1 and mult2, respectively. Details on the frequencies, magnitudes, and phases of the tones comprising the mult1 and mult2 signals are reported in Table VIII. To characterize the component response for the typical operating working condition, three signals with different amplitudes have been used for the R_1, L_1, and C_1 components. The difference between the measured and nominal values is significant for all the passive filter parameters (always greater than 20%). Since the reliability of measurement results is granted by the very low value assumed in all tests by the error parameter Err, the measured values, rather than the nominal values of the passive component parameters, should be used to calculate the passive filter impedance as well as all the other parameters that are relevant for the filter active part configuration.

V. CONCLUSION

The investigation of two case studies has been proposed to demonstrate the importance of passive R, L, and C component characterization in nonsinusoidal operating conditions. The measurement procedure proposed by the authors allowed a reliable evaluation of the R, L, and C component values of both the LISN and hybrid filters in their actual nonsinusoidal working conditions. The significant differences between the nominal and measured parameters confirm the need for methods like this. Further steps will concern the real-time implementation of the proposed measurement procedure, which could be very useful in providing active filters with self-tuning capabilities.

REFERENCES

[1] L. S. Czarnecki and Z. Staroszczyk, "On-line measurement of equivalent parameters for harmonic frequencies of a power distribution system and load," *IEEE Trans. Instrum. Meas.*, vol. 45, no. 2, pp. 467–472, Apr. 1996.

[2] J.-T. Hsu and K. D. T. Ngo, "Behavioral modeling of the IGBT using the Hammerstein configuration," *IEEE Trans. Power Electron.*, vol. 11, no. 6, pp. 746–753, Nov. 1996.

[3] M. Suzuki, S. Shibata, A. Itoh, and N. Yoshimura, "Analysis of ceramic varistor," in *Proc. 3rd Int. Conf. Properties Appl. Dielectr. Mater.*, Tokyo, Japan, Jul. 1991, pp. 655–658.

[4] P. Marino, V. Mungiguerra, F. Russo, and F. Vasca, "Parameter and state estimation for induction motors via interlaced least squares algorithm and Kalman filter," in *Proc. IEEE PESC*, 1996, vol. 2, pp. 1235–1241.

[5] H. Rasmussen, M. Knudsen, and M. Tonnes, "Parameter estimation of inverter and motor model at standstill using measured currents only," in *Proc. IEEE ISIE*, 1996, vol. 1, pp. 331–336.

[6] R. J. A. Gorter, A. Veltman, and P. P. J. Van der Bosch, "Skin effect impact on induction motor parameters estimation using an output-error identification method," in *Proc. IEEE PESC*, 1994, vol. 1, pp. 763–768.

[7] F.-Y. Shih and D.Y. Chen, "A procedure for designing EMI filters for AC line applications," *IEEE Trans. Power Electron.*, vol. 11, no. 1, pp. 170–181, Jan. 1996.

[8] L. Ferrigno, C. Liguori, and A. Pietrosanto, "Measurements for the characterization of passive components in non-sinusoidal conditions," *IEEE Trans. Instrum. Meas.*, vol. 51, no. 6, pp. 1252–1258, Dec. 2002.

[9] L. Ljung, *System Identification: Theory for the User*. Englewood Cliffs, NJ: Prentice-Hall, 1987.

[10] BIPM, IEC, IFCC, ISO, IUPAC, IUPAP, OIML, *Guide to the Expression of Uncertainty in Measurement*, 1995.

[11] M. Nave, *Line Impedance Stabilization Networks: Theory and Use*, pp. 54–56, 1985. RFI/EMI corner.

[12] FCC, *Methods of Measurement of Radio Noise Emissions From Computing Devices*, 1987. FCC/OST MP-4.

[13] *Specification for Radio Disturbance and Immunity Measuring Apparatus and Methods*, CISPR 16-1, 1998.

[14] K. Hall, "Unspecified LISN parameters can cause emissions to appear greater than 10 dB high," in *Proc. IEEE Int. Symp. Electromagn. Compat.*, 1991, pp. 474–480.

[15] J. C. Crebier, J. Roudet, and J. L. Schanen, "Problems using LISN in EMI characterization of power electronic converters," in *Proc. 30th Annu. IEEE PESC*, 1999, vol. 1, pp. 307–312.

[16] P. Tomasin, A. Zuccato, and D. Florean, "Undesired uncertainty in conducted full-compliance measurements: A proposal for verification of conformity of LISN parameters according to the requirements of CISPR16-1," in *Proc. IEEE Int. Symp. EMC*, 2001, vol. 1, pp. 7–12.

[17] G. Betta, D. Capriglione, M. Laracca, and G. Tomasso, "Reproducibility and uncertainty of conducted emission measurements for adjustable speed electrical power drive characterization," in *Proc. 21th IEEE IMTC*, May 2004, vol. 3, pp. 2120–2125.
[18] S. Bhattacharya, P. T. Cheng, and D. M. Divan, "Hybrid solutions for improving passive filter performance in high power applications," *IEEE Trans. Ind. Appl.*, vol. 33, no. 3, pp. 732–747, May/Jun. 1997.
[19] F. B. Libano, D. S. L. Simonetti, and J. Uceda, "Frequency characteristics of hybrid filter system," in *27th Annu. IEEE PESC Conf. Rec.*, 1996, vol. 2, pp. 1142–1148.
[20] D. Rivas, L. Moran, J. W. Dixon, and J. R. Espinoza, "Improving passive filter compensation performance with active techniques," *IEEE Trans. Ind. Electron.*, vol. 50, no. 1, pp. 161–170, Feb. 2003.

Luigi Ferrigno (M'04) was born in Italy in 1972. He received the M.S. degree in electronic engineering from the University of Salerno, Salerno, Italy, in 1998 and the Ph.D. degree in electrical engineering from the University of Napoli, Napoli, Italy, in 2002.

Since 2001, he has been an Assistant Professor of electrical and electronic measurements with the University of Cassino, Cassino, Italy. Since 2004, he has been the Head of the Laboratorio di Misure Industriali, Department of Automation, Electromagnetism, Information Engineering, and Industrial Mathematics (DAEIMI), University of Cassino. His current research interests include the measurement system for nondestructive testing via eddy current, wireless systems and wireless sensor network realization and characterization, and methods and instruments for the characterization of passive components and ac mains in nonsinusoidal conditions.

Marco Laracca (M'06) was born in Formia, Italy, in 1973. He received the M.S. degree in electrical engineering and the Ph.D. degree in electrical and information engineering from the University of Cassino, Cassino, Italy, in 2002 and 2006, respectively.

Since February 2006, he has been an Assistant Professor of electrical and electronic measurements with the University of Cassino. His current research interests include the realization of measurement systems for nondestructive testing via eddy current, sensor realization and characterization, power quality measurements, and electric power measurement under nonsinusoidal conditions.

Antonio Pietrosanto (M'99) was born in Napoli, Italy, in 1961. He received the M.S. and Ph.D. degrees in electrical engineering from the University of Napoli in 1986 and 1990, respectively.

He became an Assistant Professor in 1991 and an Associate Professor of electrical and electronic measurements in 1999 with the University of Salerno, Salerno, Italy, where, November 2001, he has been a Full Professor of electrical and electronic measurements. His scientific interests include instrument fault detection isolation and accommodation, digital signal and image processing for real-time diagnostic and process control, and fiber-optic sensors.